Journal of Fluorescence, Vol. 7, No. 1, 1997

Time-Gated Microscopic Energy Transfer Measurements for Probing Mitochondrial Metabolism

Herbert Schneckenburger,[1–3] Michael H. Gschwend,[1] Wolfgang S. L. Strauss,[1] Reinhard Sailer,[1] and Rudolf Steiner[1]

Received June 14, 1996; accepted September 27, 1996

Spectroscopic and microscopic methods for probing mitochondrial malfunction were established using cultivated endothelial cells from the calf aorta and various inhibitors of the respiratory chain, which is located at the inner mitochondrial membrane. Time-gated fluorescence spectroscopy was used to measure autofluorescence of the coenzyme NADH as well as "energy transfer efficacy" from excited NADH molecules (energy donor) to the mitochondrial marker rhodamine-123 (energy acceptor). Autofluorescence usually exhibited a weak increase after specific inhibition of enzyme complexes of the respiratory chain. In contrast, a pronounced increase in energy transfer efficacy was observed after inhibition of the same enzyme complexes. The detection of donor (NADH) and acceptor (R123) fluorescence in different nanosecond time gates following the exciting laser pulses enhances selectivity and improves quantification of energy transfer measurements. Therefore, time-gated energy transfer spectroscopy is suggested to be an appropriate tool for probing mitochondrial malfunction.

KEY WORDS: Time-gated fluorescence spectroscopy; energy transfer; NADH; rhodamine-123; mitochondrial malfunction.

INTRODUCTION

An increasing number of diseases such as mitochondrial myopathies[1–5] and neurodegenerative diseases[5–9] have been related to malfunction of the mitochondrial respiratory chain. Detection and characterization of mitochondrial deficiencies often require complex biochemical procedures after cell lysis. In contrast, fluorescence techniques are nondestructive and suitable to detect various metabolites in living cells and tissues, e.g., the coenzymes nicotinamide adenine dinucleotide in its reduced form (NADH)[10,11] and flavin mononucleotide (FMN) or dinucleotide (FAD) in its oxidized form.[11–13] NADH and flavin molecules are both involved in redox reactions occurring within the cytoplasm or organelles, e.g., mitochondria. If electron transfer within the respiratory chain, which is located at the inner mitochondrial membrane, is inhibited, the oxidation of NADH is impeded. However, due to an overlap of the emission bands of mitochondrial NADH and flavins,[11,14,15] as well as a superposition by cytoplasmatic fluorophores, quantification of mitochondrial malfunction becomes difficult. Therefore, to enhance the specificity of detection of mitochondrial NADH and flavins, two methods were established:

(i) time-gated fluorescence detection of individual components with different lifetimes of their excited singlet state, using short laser pulses for excitation and variable nanosecond time gates for detection; and

[1] Institut für Lasertechnologien in der Medizin und Messtechnik an der Universität Ulm, Helmholtzstr. 12, D-89081 Ulm, Germany.
[2] Fachhochschule Aalen, Optoelektronik, D-73428 Aalen, Germany.
[3] To whom correspondence should be addressed at Fachhochschule Aalen, Optoelektronik, Postfach 1728, D-73428 Aalen, Germany.

1053-0509/97/0300-0003$12.50/0

(ii) energy transfer measurements from the excited states of NADH to the mitochondrial marker rhodamine-123 (R123).

Usually, NADH occurs in two conformations—an extended conformation when it is bound to proteins and a folded conformation within an aqueous environment ("free" NADH).[16,17] Both species exhibit overlapping emission bands with maxima around 440 and 465 nm and distinctly different fluorescence lifetimes of about 2 and 0.4–0.6 ns, respectively.[15,16,18] Using the method of time-gated fluorescence spectroscopy, free and protein-bound NADH could be detected almost selectively in different time gates. This method of detection was used to establish a correlation between the fluorescence intensity of free NADH and the oxygen concentration.[19]

To establish the method of energy transfer spectroscopy, cultivated endothelial cells were incubated with nontoxic concentrations of the mitochondrial marker R123[20,21] and toxic concentrations of well-known inhibitors of enzyme complexes of the respiratory chain. Cellular emission spectra were recorded in various time gates following the excitation pulse. The fluorescence intensities of NADH (energy donor) and R123 (energy acceptor) were determined in appropriate time gates where spectral overlap was as low as possible. As shown in a recent article,[22] the quantum ratio of acceptor and donor fluorescence Q_A/Q_D increases linearly with the acceptor concentration c_A as well as with the concentration-independent energy transfer rate $k_{ET}^{(0)}$. Since the intensity ratio I_{R123}/I_{NADH} of R123 and NADH fluorescence is proportional to Q_A/Q_D, the relation $I_{R123}/(I_{NADH}c_{R123})$ is suggested to be an appropriate measure of energy transfer efficacy.

MATERIALS AND METHODS

Chemicals

Inhibitors of the respiratory chain (rotenone, antimycin, and oligomycin) were obtained from Sigma (Deisenhofen, Germany) and were dissolved without further purification in ethanol. Stock solutions with final concentrations of 10^{-3} *M* (rotenone) or $5 \cdot 10^{-3}$ *M* (antimycin, oligomycin) were prepared. Rhodamine 123 (R123) was obtained from Fluka (Neu-Ulm, Germany) and used without further purification. Stock solutions were prepared in distilled water with a final concentration of 10^{-3} *M* and sterilized by filtration using a 0.2-μm-pore filter.

Cell Cultures

In vitro experiments were carried out using BKEz-7 endothelial cells from the calf aorta, which were established by Dr. W. Halle, Institut für molekulare Pharmakologie, Berlin.[23] Cells were routinely cultivated on microscopic slides in minimum essential medium (MEM) supplemented with 5% fetal calf serum (FCS), glutamine (2 m*M*), and antibiotics (penicillin, streptomycin) at 37°C and 5% CO_2. After a growing period of 36 h almost confluently growing cells were obtained. Autofluorescence was measured after incubation for 30 min with various inhibitors of the mitochondrial respiratory chain and subsequent rinsing with phosphate-buffered saline (PBS). Complex I (NADH–coenzyme Q reductase) was inhibited with rotenone (1 μ*M*). The electron transport in complex III (coenzyme QH_2–cytochrome *c* reductase) or complex V (ATP synthase) was disrupted using antimycin (5 μ*M*) or oligomycin (5 μ*M*), respectively. Control measurements were carried out with nonincubated cells. For energy transfer spectroscopy cells were incubated for 30 min with noncytotoxic concentrations of R123 (25 μ*M*) or coincubated with R123 (25 μ*M*) and the various inhibitors (see above). Evaluation of the cytotoxicity of the inhibitors or R123 is described in detail elsewhere.[22] The applied concentrations of inhibitors resulted in 50% cell survival after an additional growth period of 48 h. Measurements of the intracellular amount of R123 are also described in Ref. 22.

Time-Resolved Fluorescence Spectroscopy

Fluorescence decay kinetics were used to determine the appropriate time gates for almost-selective detection of NADH or R123. Mitochondrial malfunction was probed by nanosecond time-gated fluorescence spectroscopy. Autofluorescence was measured in the time gate 0–5 ns and evaluated at the emission maximum of free NADH (465 nm). For energy transfer spectroscopy, fluorescence spectra were recorded in the range of 415–600 nm within the time gates 0–5 and 5–10 ns, i.e., during and after the exciting laser pulse. Fluorescence intensities at the emission maxima of NADH (465 nm; time gate, 0–5 ns) and R123 (530 nm; time gate, 5–10 ns) were determined separately. As a measure of energy transfer efficacy, the ratio of fluorescence intensities of acceptor (I_{R123}) and donor (I_{NADH}), divided by the intracellular concentration of R123 (c_{R123}), was calculated. For descriptive statistical analysis, robust statistical measures (trimmed mean, adjusted and trimmed standard deviations) were used.[24] Robust measures of location

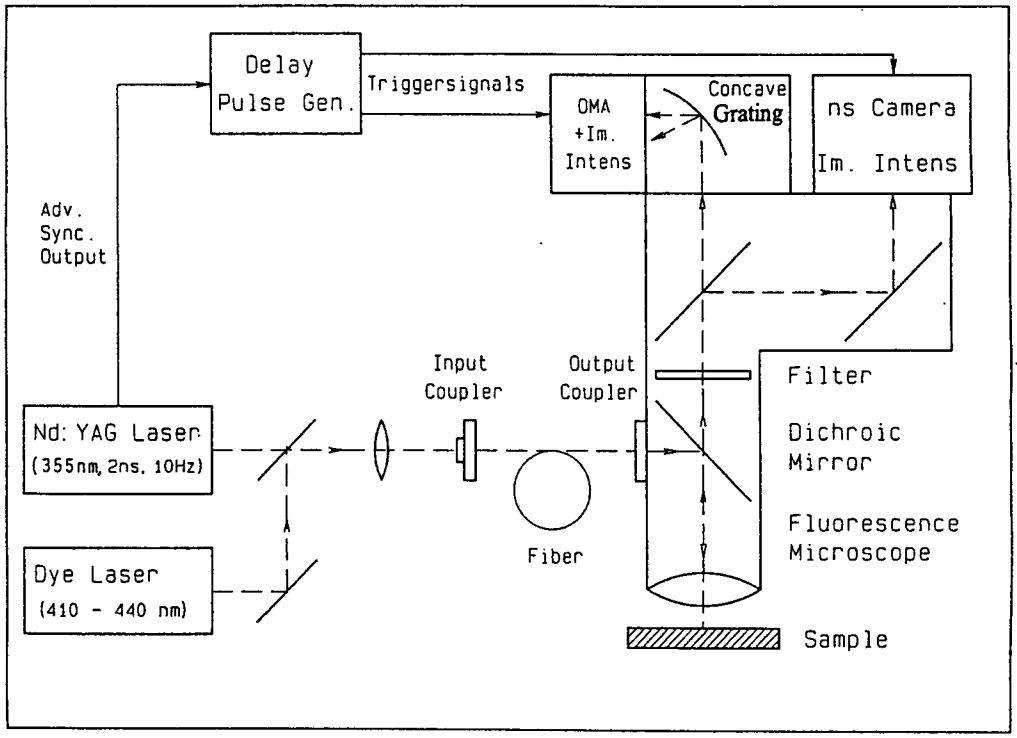

Fig. 1. Experimental setup for time-gated fluorescence spectroscopy and imaging of microscopic samples (reproduced from Ref. 26 with modifications).

and dispersion for the quotient of three random variables $I_{R123}/(I_{NADH}c_{R123})$ were calculated assuming stochastical independence of these variables. Pairwise comparisons (three for energy transfer and three for autofluorescence) were tested at a significance level 5/3% each, as described further in Ref. 22.

Fluorescence decay kinetics were recorded using a frequency-doubled laser diode (PLP01; Hamamatsu Photonics) at 390 nm (pulse energy, 10 fJ; pulse duration, 40 ps; repetition rate, 1 MHz), appropriate long-pass filters ($\lambda \geq 435$ nm) or band-pass filters (λ = 430–475 or 505–565 nm) for fluorescence detection, a highly sensitive photomultiplier (R928; Hamamatsu Photonics) together with a photon counting equipment (Tennelec, USA) and an optical multichannel analyzer. Fluorescence decay curves were reconvoluted and fitted with commercial programs for two or three-exponential components (IBH, Edinburgh Instruments, UK). Time resolution was about 200 ps. Details have been described previously.[25]

The apparatus for time-gated emission spectroscopy and imaging is shown in Fig. 1. Microscopic slides were illuminated by the third harmonic of a Nd:YAG laser in the Q-switch mode (DCR 11; Spectra Physics; λ_{ex} = 355 nm; pulse energy, attenuated to 0.24 mJ; pulse duration, 2 ns; repetition rate, 10 Hz). The laser was coupled to the microscope via fiber optics. An image of an area of 0.0125 mm^2 of incubated cells (containing 5–10 cells) was formed on the entrance slit of a purpose-made polychromator, which was used in combination with an optical multichannel analyzer (IMD C4562; Hamamatsu Photonics). The image intensifier of IMD C4562 was triggered by the laser pulse using appropriate synchronization electronics. Therefore, time gates of 5 ns with variable delay times could be adjusted. Emission spectra were integrated on the detector array over 200 laser pulses, corresponding to an overall exposure of 3.2 J·cm^{-2} during each measurement, which was below the limit of phototoxicity of R123 (about 10 J/cm^2).[22] Spectral resolution was about 5 nm. For all measurements, background luminescence resulting from the microscope optics after *uv* excitation was subtracted. During NADH detection, this background luminescence was up to 50% of the measured signal within the time gate 0–5 ns, up to 60% within the time gate 5–10 ns, and up to 95% for continuous wave (cw) detection (using the 365-nm band of a mercury high-pressure lamp for excitation). When R123 was measured, background luminescence was about 25% within the time gate 0–5 ns, about 15% within the time gate 5–10 ns, and up to 100% for cw

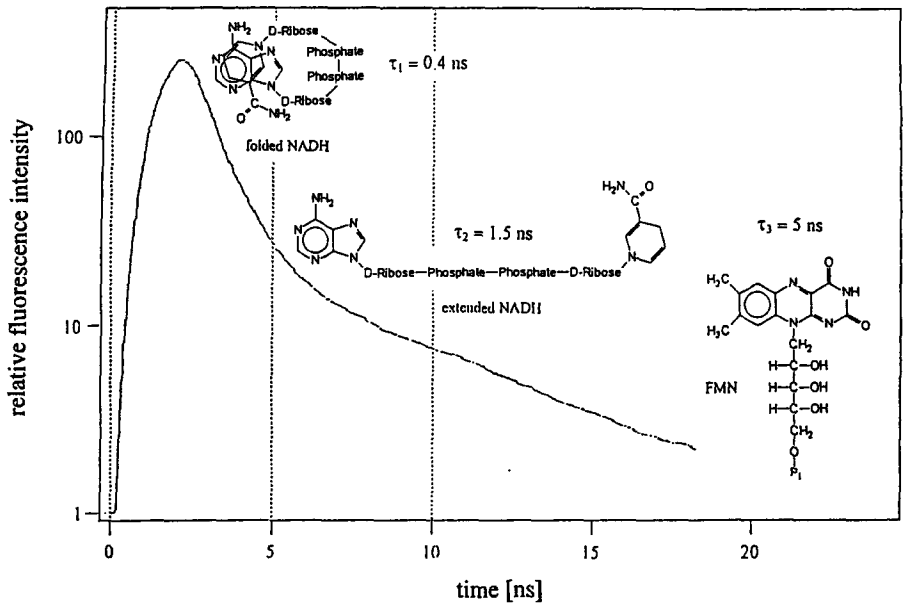

Fig. 2. Decay kinetics of autofluorescence of BKEz-7 endothelial cells from calf aorta (λ_{ex} = 390 nm; $\lambda_{em} \geq$ 435 nm). Relevant fluorophores and time gates for detection (0–5, 5–10 ns) are indicated.

detection. This considerable luminescent background justifies the time-gated fluorescence measurements as mentioned above.

Additional components of the equipment (Fig. 1) are a dye laser (PDL-1; Spectra Physics; λ_{ex} = 410–440 nm)—pumped by the third harmonic of the Nd:YAG laser—and an ultrafast videocamera (NCA; Proxitronic; sensitivity, 5 μlux). This camera permits fluorescence detection within 5-ns time gates at adjustable delay times. Images resulting from individual laser pulses are kept in a sample-and-hold unit until the subsequent laser pulse. These images are recorded on videotape and—for contrast enhancement—integrated off-line up to 10 s. Further details and a summary of applications of time-gated fluorescence imaging and spectroscopy are given in a recent article.[26]

RESULTS

Fluorescence Decay Kinetics

The decay curve of intrinsic fluorescence of BKEz-7 endothelial cells ($\lambda \geq$ 435 nm) is shown in Fig. 2. This curve can be fitted by a sum of three exponentially decaying components with lifetimes of T_1 = 0.5 ± 0.15 ns, T_2 = 2.0 ± 0.5 ns, and T_3 = 5–6 ns. In agreement with literature data[12,16,18] these time constants were attributed to free and protein-bound NADH as well as to flavin molecules, respectively. After incubation of the BKEz-7 cells with rhodamine-123, the same lifetime T_1 was detected, whereas T_2 was not resolved. The fluorescence lifetime of the long-lived component was 4.5 ± 0.3 ns, which corresponds to the decay time of R123 in aqueous solution.[22] Flavin fluorescence of similar lifetime (T_3) was superimposed by the much more pronounced R123 signal and therefore not resolved in this case. In the spectral range of 430–475 nm, only T_1 and T_2 were detected. Within the limits of error these lifetimes did not change after incubation with R123. In Fig. 2 the time gates of 0–5 and 5–10 ns are indicated, which proved to be the most appropriate for almost-selective detection of (free) NADH and R123, respectively.

Time-Gated Fluorescence Spectroscopy

Autofluorescence of Endothelial Cells. Time-gated spectra of intrinsic fluorescence (recorded at 0–5 ns; Fig. 3) showed a broad emission band with a maximum around 465 nm and a shoulder at about 520 nm, which were attributed to free NADH and flavin molecules, respectively. Inhibition of the mitochondrial respiratory chain by antimycin (enzyme complex III) resulted in an increase in fluorescence by a factor of 1.2–1.3, and inhibition by rotenone (enzyme complex I) in an increase by a factor of 1.3–1.5, compared with untreated control cells. A quantitative evaluation of NADH emission (465 nm) over 17–30 individual measurements in each case

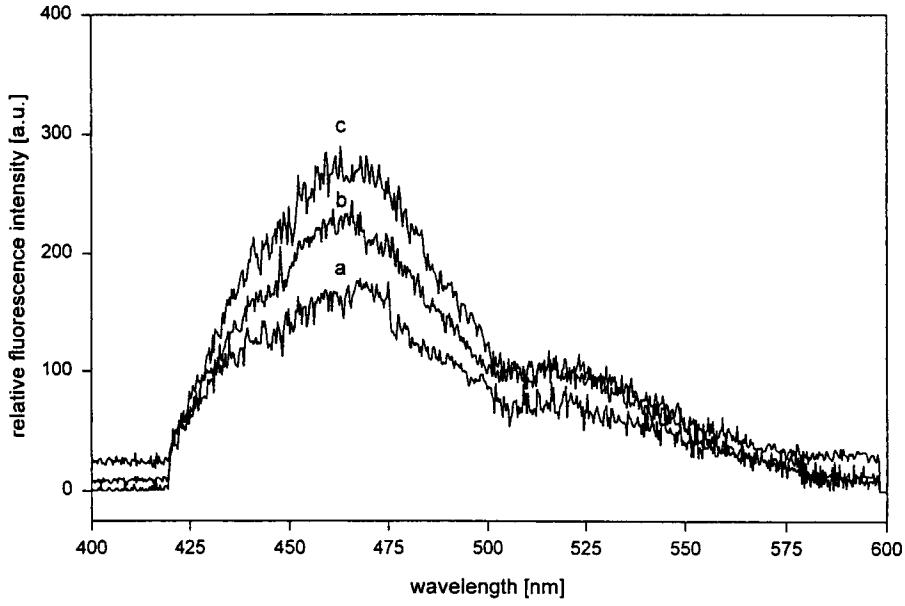

Fig. 3. Time-gated emission spectra of autofluorescence of BKEz-7 endothelial cells from calf aorta (time gate, 0–5 ns; λ_{ex} = 355 nm): (a) untreated cells; (b) inhibition of enzyme complex III with antimycin (5 μ*M*, 30 min); (c) inhibition of enzyme complex I with rotenone (1 μ*M*, 30 min).

Table I. Intensity of Autofluorescence I_{NADH} (Photon Counts) and "Energy Transfer Efficacy" $I_{R123}/(I_{NADH}c_{R123})$ (Arbitrary Units) of BKEz-7 Endothelial Cells After Inhibition of Enzyme Complexes of the Mitochondrial Respiratory Chain in Comparison with Untreated Control Cells

Inhibitor	I_{NADH}	$I_{R123}/(I_{NADH}c_{R123})$
None	135 ± 69	145 ± 91
Rotenone (enzyme complex I)	174 ± 74	587 ± 398
Antimycin (enzyme complex III)	157 ± 84	255 ± 137
Oligomycin (enzyme complex V)	121 ± 80	283 ± 153

showed an increase in the mean value by a factor of 1.3 after incubation with rotenone, an increase by a factor of about 1.15 after incubation with antimycin, and a slight decrease (factor 0.9) after incubation with oligomycin (inhibitor of enzyme complex V) compared with nonincubated control cells (79 measurements). Robust mean values and corresponding robust standard deviations are listed in Table I.

Energy Transfer Spectroscopy. Fluorescence spectra of BKEz-7 endothelial cells incubated with R123 and BKEz-7 cells coincubated with R123 and antimycin, measured in the time gate of 0–5 or 5–10 ns, are shown in Figs. 4 and 5. Broad emission bands with maxima around 465 and 530–535 nm, corresponding to (free) NADH and R123, are clearly resolved. Flavin emission (maximum around 520 nm) is superimposed on the R123 band but is more than 10 times weaker. In comparison with the rhodamine band, NADH fluorescence becomes very low in the time gate 5–10 ns. Therefore, fluorescence of R123 can be evaluated with very little superimposition by NADH within this time gate (Fig. 5). Inversely, the fluorescence intensity of NADH can be determined almost without superimposition by R123 within the time gate 0–5 ns (Fig. 4). A slight increase in NADH emission and a more pronounced increase in the fluorescence of R123 (by a factor of about 2) were observed after mitochondrial inhibition by antimycin. The quantitative evaluation of R123 (time gate, 5–10 ns) and NADH (time gate, 0–5 ns) intensities was carried out for cells coincubated with R123 and one of the inhibitors of the enzyme complex I, III, or V (20–33 individual measurements in each case), as well as for control cells incubated solely with R123 (83 measurements). Intracellular rhodamine concentrations (determined from 8–10 measurements in each case)[22] decreased to less than 30% of the control cells after inhibition of enzyme complex I and to about 80% after inhibition of enzyme complex III, but increased to about 250% of the control cells after inhibition of enzyme complex V. The ratio $I_{R123}/(I_{NADH}c_{R123})$ ("energy transfer efficacy") was calculated in each case; robust mean values and robust standard deviations are summarized in Table I. The mean value of this ratio increased by a factor of 4 after inhibition of enzyme complex I and by a factor of about 2 after inhibition of enzyme complex III or V. Increases in energy transfer efficacies after in-

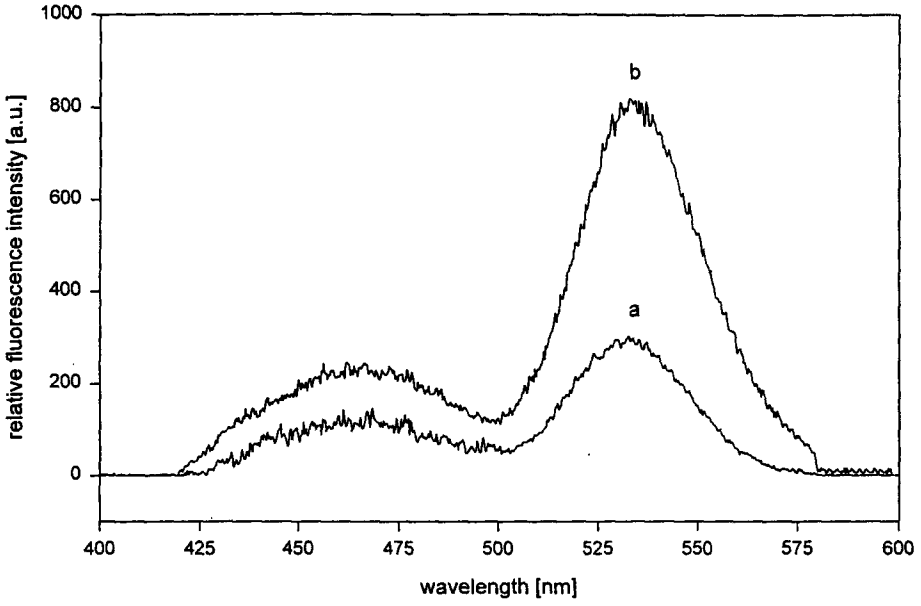

Fig. 4. Time-gated fluorescence spectra of BKEz-7 endothelial cells (time gate, 0–5 ns; λ_{ex} = 355 nm): (a) after incubation with R123 (25 μ*M*, 30 min); (b) after incubation with R123 (25 μ*M*, 30 min) and inhibition of enzyme complex III with antimycin (5 μ*M*, 30 min).

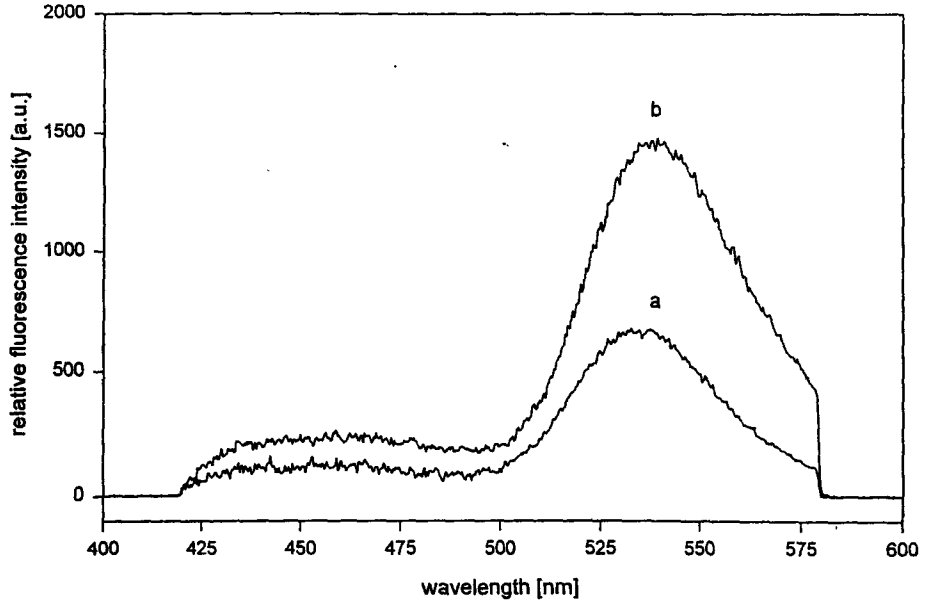

Fig. 5. Time-gated fluorescence spectra of BKEz-7 endothelial cells (time gate, 5–10 ns; λ_{ex} = 355 nm): (a) after incubation with R123 (25 μ*M*, 30 min); (b) after incubation with R123 (25 μ*M*, 30 min) and inhibition of enzyme complex III with antimycin (5 μ*M*, 30 min).

hibition of enzyme complex I, III, or V were found to be statistically significant.

DISCUSSION

As shown in Figs. 4 and 5, the fluorescence intensity of R123 increases by a factor of 2 after inhibition of enzyme complex III of the respiratory chain. A similar increase in R123 emission was recently observed in mixed solutions of NADH and R123 in phosphate-buffered saline (PBS) when, at a constant concentration of R123 (10^{-4} *M*), the concentration of NADH was increased from 10^{-4} to 10^{-3} *M*.[22] This was explained by the fact that every tenth NADH molecule transferred its excitation energy to an R123 molecule. A slight shortening of the fluorescence decay time of NADH in PBS (short-lived component: from about 0.60 ns at concentrations up to 10^{-4} *M* to 0.54 ns at a concentration of 10^{-3} *M*) in the presence of R123 indicates that this energy transfer is nonradiative and probably occurs according to the Förster mechanism.[27] In this case the total rate of deactivation of the excited molecular state is increased by the rate of energy transfer, and lifetime is reduced concomitantly. Spectral overlap of the fluorescence of the donor (NADH: emission maximum around 465 nm) and absorption of the acceptor (R123: excitation maximum around 475 nm)—as required by the Förster model—is sufficiently fulfilled. So far, no shortening of fluorescence lifetimes was detected for cultivated cells, which may be due to the large deviations of decay times inherently related to cellular experiments.

It was recently shown that the quantum ratio Q_A/Q_D of acceptor and donor fluorescence increases linearly with the acceptor concentration c_A and with the energy transfer rate $k_{ET}^{(0)}$.[22] Since the intensity ratio I_{R123}/I_{NADH} is proportional to Q_A/Q_D, this implies that $k_{ET}^{(0)}$ increases after mitochondrial inhibition. Although $k_{ET}^{(0)}$ is independent of c_A, it may depend on the concentration of the donor, since energy transfer from donor to acceptor molecules (NADH → R123)—as well as from one donor to another one (NADH → NADH)—is proportional to the sixth power of their intermolecular distance.[27] Therefore, the increase in the mean value of $I_{R123}/(I_{NADH}c_{R123})$ by a factor of 4 after inhibition of enzyme complex I or by a factor of about 2 after inhibition of enzyme complex III or V indicates that the concentration of reduced NADH is increased after mitochondrial inhibition.

As documented in Table I, changes in the mean values of autofluorescence (NADH) after inhibition of enzyme complex I, III, or V of the repiratory chain are smaller than the standard deviations obtained for each enzyme complex and are statistically *not* significant. In contrast, changes in energy transfer efficacy $I_{R123}/(I_{NADH}c_{R123})$ due to mitochondrial inhibition are pronounced and statistically significant, thus proving the high selectivity of energy transfer spectroscopy for probing mitochondrial metabolism. *Time-gated emission spectroscopy* improves the selective detection of donor and acceptor fluorescence, since a minimum of spectral overlap is attained by the selection of different time gates. In addition, only by time-gated detection can the large luminescent background resulting from various components of the microscope system (decay times above 50 ns) be reduced significantly.

Time-gated emission spectroscopy can be combined well with time-gated fluorescence imaging (as shown in Fig. 1) for diagnosis of mitochondrial malfunction in various kinds of diseases. For future applications, time-consuming measurements of intracellular dye concentrations should be avoided. According to the literature, the mitochondrial uptake of R123 depends on the membrane potential.[20,21] Therefore, the use of alternative energy acceptors whose accumulation is independent from biophysical/biochemical parameters is desirable. Alternatively, a spectroscopic determination of acceptor concentrations in living cells may also be useful.

ACKNOWLEDGMENTS

The authors thank M. Bauer for his cooperation in the experiments, M. Kron and U. Steeb (Department of Biometry and Medical Documentation, University of Ulm) for their statistical evaluation, and C. Hintze and R. Martin for their skillful technical assistance. Financial support by the Bundesministerium für Bildung, Wissenschaft, Forschung und Technologie (BMBF; Grant 13N6308/0) is gratefully acknowledged.

REFERENCES

1. S. DiMauro, E. Bonilla, M. Zeviani, M. Nakagawa, and D. C. DeVivo (1985) *Ann. Neurol.* **17**, 521–526.
2. R. A. Capaldi (1988) *TIBS* **13**, 144–148.
3. D. C. Wallace (1992) *Annu. Rev. Biochem.* **61**, 1175–1212.
4. R. Luft (1994) *Proc. Natl. Acad. Sci. USA* **91**, 8731–8738.
5. M. J. Jackson, J. A. Schaefer, M. A. Johnson, A. A. M. Morris, D. M. Turnbull, and L. A. Bindoff (1995) *Brain* **118**, 339–357.
6. A. H. V. Schapira (1994) *Move. Disord.* **9**, 125–138.
7. W. D. Parker, N. J. Mahr, C. M. Filley, J. K. Parks, D. Hughes, D. A. Young, and C. M. Cullum (1994) *Neurology* **44**, 1086–1090.
8. M. Hasitz, Z. Rácz, A. Nagy, and A. Lipcsey (1995) *Arch. Gerontol. Geriatr.* **21**, 53–61.

9. M. W. J. Cleeter, J. M. Cooper, V. M. Darley-Usmar, S. Moncada, and A. H. V. Schapira (1994) *FEBS Lett.* **345**, 50–54.
10. T. Galeotti, G. D. V. VanRossum, D. H. Mayer, and B. Chance (1970) *Eur. J. Biochem.* **17**, 485–496.
11. J.-M. Salmon, E. Kohen, P. Viallet, J. G. Hirschberg, A. W. Wouters, C. Kohen, and B. Thorell (1982) *Photochem. Photobiol.* **36**, 585–593.
12. P. Galland and H. Senger (1988) *J. Photochem. Photobiol. B Biol.* **1**, 277–294.
13. M. Nokubo, I. Zs-Nagy, K. Kitani, and M. Ohta (1988) *Biochim. Biophys. Acta* **939**, 441–448.
14. B. Chance, P. Cohen, F. F. Jöbsis, and B. Schoener (1962) *Science* **137**, 499–502.
15. J. R. Lakowicz (1983) *Principles of Fluorescence Spectroscopy*, Plenum Press, New York, London.
16. T. G. Scott, R. D. Spencer, N. J. Leonard, and G. Weber (1970) *J. Am. Chem. Soc.* **92**, 687–695.
17. P. L. Luisi, A. Baici, F. J. Bonner, and A. Aboderin (1975) *Biochemistry* **14**, 362–368.
18. H. Schneckenburger and K. König (1992) *Opt. Eng.* **31**, 1447–1451.
19. R.-J. Paul and H. Schneckenburger (1996) *Naturwissenschaften* **83**, 32–35.
20. L. V. Johnson, M. L. Walsh, and L. B. Chen (1980) *Proc. Natl. Acad. Sci. USA* **77**, 990–994.
21. T. Horikoshi, T. Yoshioka, Y. Kubota, and K. Yanagisawa (1987) *Cell Struct. Funct.* **12**, 525–537.
22. H. Schneckenburger, M. H. Gschwend, W. S. L. Strauss, R. Sailer, M. Kron, U. Steeb, and R. Steiner, submitted for publication.
23. W. Halle, W.-E. Siems, K. D. Jentzsch, E. Teuscher, and E. Görres (1984) *Die Pharmazie* **39**, 77–81.
24. J. Högel, J. Schmid, and W. Gaus (1994) *Biom. J.* **36**, 411–427.
25. H. Schneckenburger, W. Strauss, A. Rück, H. K. Seidlitz, and J. M. Wessels (1992) *Opt. Eng.* **31**, 995–999.
26. H. Schneckenburger, K. König, T. Dienersberger, and R. Hahn (1994) *Opt. Eng.* **33**, 2600–2606.
27. T. Förster (1960) *Z. Elektrochem.* **64**, 157–165.